Available online at www.sciencedirect.com
ScienceDirect
Journal of Photochemistry and Photobiology A: Chemistry 195 (2008) 330–336
Journal of Photochemistry and Photobiology A:Chemistry
www.elsevier.com/locate/jphotochem

Photodissociation dynamics of OCS and CS_2 adsorbed on water ice films at 193 nm

Atsushi Ikeda, Noboru Kawanaka, Akihiro Yabushita, Masahiro Kawasaki *

Department of Molecular Engineering, Kyoto University, Kyoto 615-8510, Japan

Received 16 June 2007; received in revised form 25 September 2007; accepted 29 October 2007
Available online 17 November 2007

Abstract

Photodissociation dynamics of OCS and CS_2 adsorbed on water ice films at 90 K was investigated at 193 nm by measuring the time-of-flight spectra of photodissociated S(^{1}D) and S(^{3}P) atoms. The translational energy distributions are well represented by a combination of Gaussian and Maxwell–Boltzmann (M–B) distributions corresponding to the fast and slow time-of-flight components, respectively. Formation of the sulfur dimer on the ice surface is proposed as a secondary photoproduct. The fine-structure branching ratios of S(^3P_J) from OCS and CS_2 adsorbed on H_2O or D_2O water ice films were also determined.

Keywords: Carbonyl sulfide; Carbon disulfide; Ice surface; Heterogeneous reaction; Photodissociation dynamics

1. Introduction

Chemistry occurring on water ice surfaces has received increasing attention in recent years since ice surfaces are a unique reaction environment as compared to the liquid or gas phase. For example, chemical processes on ice surfaces will play an important role in astrochemistry. Sulfur-containing compounds are common in planetary atmospheres and comets covered by ice [1]. Grim and Greenberg reported sulfur dimer formation as a result of the photolysis of H_2S on ices [2]. A'Hearn et al. detected S_2 during the chemical analysis of comet contents and found its concentration was correlated to CS concentration [3].

In the gas phase, OCS dissociates primarily via a singlet channel into CO + S(^{1}D) by photoirradiation at 190–255 nm [4–6]. The translational energy distribution of S(^{1}D) atoms is observed to be bimodal. A minor contribution by the triplet channel, Reaction 2, was reported by Katayanagi et al. [5]. The calculated reaction enthalpies are reported below [7].

$$\mathrm{OCS} \rightarrow \mathrm{CO} + \mathrm{S}(^1\mathrm{D}), \quad \Delta H = 100\,\mathrm{kcal/mol} \tag{1}$$

$$\mathrm{OCS} \rightarrow \mathrm{CO} + \mathrm{S}(^3\mathrm{P}_2), \quad \Delta H = 74\,\mathrm{kcal/mol} \tag{2}$$

During the 222 nm photodissociation of OCS adsorbed on an LiF (0 0 1) substrate at 116 K, formation and branching ratios of S(^{3}P and ^{1}D) and CO were reported by Leggett et al. [8] and Dixon-Warren et al. [9]. The sulfur-product branching ratio [S(^{3}P)]/[S(^{1}D)], shifted from nearly zero in the gas phase to three, the theoretical upper limit, in the adsorbed state [8]. The translational energy distribution of S(^{3}P) was well represented by a Maxwell–Boltzmann (M–B) distribution with an average translational energy of 3.0–4.2 kcal/mol over a range of surface coverage, 10^{-4} to 0.1 ML. The sulfur dimer was produced by the reaction of a triplet sulfur atom with a coadsorbed OCS molecule on the cold substrate [9]. Sulfur dimer formation has also been observed during photolysis of $(OCS)_n$ clusters [4] and under slow flow conditions [10].

$$\mathrm{S}(^1\mathrm{D}) + \mathrm{OCS} \rightarrow \mathrm{S_2} + \mathrm{CO}, \quad \Delta H = -54\,\mathrm{kcal/mol} \tag{3}$$

$$\mathrm{S}(^3\mathrm{P}_2) + \mathrm{OCS} \rightarrow \mathrm{S_2} + \mathrm{CO}, \quad \Delta H = -28\,\mathrm{kcal/mol} \tag{4}$$

The following photodissociation processes of gas-phase CS_2 have been reported by various groups [11–13].

$$\mathrm{CS_2} \rightarrow \mathrm{CS} + \mathrm{S}(^1\mathrm{D}), \quad \Delta H = 131\,\mathrm{kcal/mol} \tag{5}$$

$$\mathrm{CS_2} \rightarrow \mathrm{CS} + \mathrm{S}(^3\mathrm{P}_2), \quad \Delta H = 105\,\mathrm{kcal/mol} \tag{6}$$

* Corresponding author. Tel.: +81 75 383 2572; fax: +81 75 383 2573.
E-mail address: kawasaki@photon.mbox.media.kyoto-u.ac.jp (M. Kawasaki).

1010-6030/$ – see front matter © 2007 Elsevier B.V. All rights reserved.
doi:10.1016/j.jphotochem.2007.10.023

The product branching ratio for reactions (5) and (6) [S(^{3}P)]/[S(^{1}D)], was 1.6 at 193 nm. The triplet dissociation channel is opened via the photoprepared $^1B_2$ state. No studies have been reported on the photodissociation of surface-bound CS_2.

In this study, the photodissociation dynamics of OCS and CS_2 adsorbed on water ice films is monitored by measuring translational energy distributions of the photofragmented sulfur atoms. There is evidence for S_2 formation from the reaction of sulfur atoms with coadsorbed parent molecules. The isotope effect on the spin-orbit state distributions of S(^3P_J) is investigated for ice films of the water isotopomers, H_2O and D_2O.

2. Experimental

The experimental apparatus and procedures of ice film preparation have been described elsewhere [14]. Photodissociation of OCS or CS_2 adsorbed on an ice film was carried out in a vacuum chamber, which was equipped with two turbo molecular pumps in tandem. Ice films were prepared on polycrystalline Au substrates with (1 1 1) domains [15]. Two types of water ice films were used in this experiment: amorphous solid water (ASW) and polycrystalline ice (PCI) films. ASW films were prepared with the background deposition at 100 K for 60 min and 20 Torr stagnation pressure of water vapor for a pulsed gas valve. The exposure was typically 1800 L (1 L = 1×10^{-6} Torr s), which resulted in the formation of 600 ML of H_2O (or D_2O) on the Au substrate [16]. PCI films were prepared with the background deposition of water vapor at 130 K for 60 min, and then maintained at this temperature for a further 30 min for annealing purposes. The gas mixture (4%) of OCS and CS_2 with N_2 diluent was introduced into the vacuum chamber with the background deposition. A typical stagnation pressure of the pulsed gas valve for the mixture gas was 10 Torr. The chamber pressure was 4.0×10^{-8} Torr without sample gas injection. OCS or CS_2 adsorbed on ice films were photodissociated using an excimer laser (Lambda Physik, COMPex, 10 Hz, typically less than 0.3 mJ cm^{-2} pulse^{-1}) at 193 nm. Neutral sulfur atom photofragments were subsequently ionized at a distance of 3 mm from the substrate surface by [2 + 1] resonance enhanced multiphoton ionization (REMPI) on the S ($^1F_3 \leftarrow\leftarrow {}^1D_2$, $^3P_J \leftarrow\leftarrow {}^3P_J$, $J = 0, 1, 2$) transition with a lens ($f = 0.10$ m) and collected with a small TOF mass spectrometer aligned perpendicular to the ice surface. The requisite radiation for REMPI at wavelengths 288.2 nm and 308–311 nm was produced by an Nd^{3+}:YAG pumped dye laser (Lambda Physik, SCANmate, 0.2 mJ pulse^{-1} at UV) using Rhodamine 590 and Rhodamine 610 dyes, followed by subsequent frequency doubling with a KDP crystal. Time-of-flight (TOF) spectra of S atoms were measured as a function of time delay, t, between photolysis and probe pulses, which corresponds to the flight time between the substrate and the detection region. Temperature of the Au substrate was kept at 90 K during UV photoirradiation unless stated otherwise.

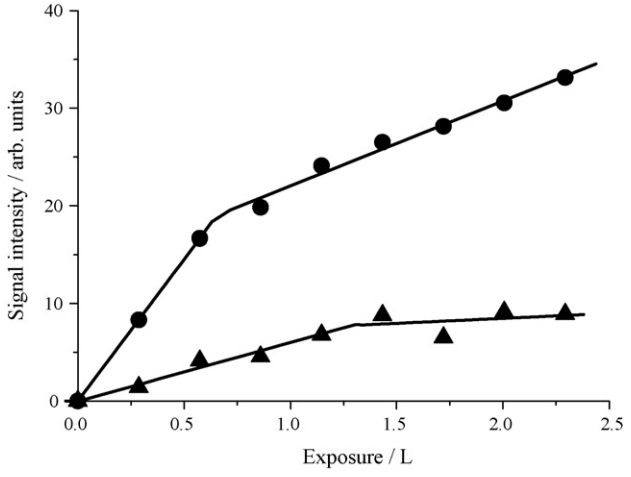

Fig. 1. Signal intensity of S($^3P_2$) atoms from the 193 nm photodissociation of OCS as a function of OCS exposure on polycrystalline ice film (circle) and amorphous one (triangle). Substrate temperature $T_S = 90$ K.

3. Results

3.1. Photodissociation of OCS adsorbed on ice films at 193 nm

3.1.1. Preparation of an OCS monolayer on ice films

Fig. 1 shows the integrated S($^3P_2$) TOF signal intensity from the 193 nm photodissociation of OCS as a function of OCS exposure (i.e. OCS surface coverage) on PCI or ASW films. The signal intensity from the PCI and ASW films increased linearly up to doses of 0.6 and 1.4 L, respectively, indicating formation of the first monolayer of OCS on the ice surface. According to Huang et al. [17] adsorption of OCS on a GaAs substrate increased linearly with OCS exposure up to 0.5 L, agreeing with our results. In the following sections, experiments were performed with one-monolayer exposures unless stated otherwise.

3.1.2. Time-of-flight spectra of S(^1D)

The upper panel of Fig. 2 shows a typical S(^{1}D) TOF spectrum obtained from the photodissociation of OCS adsorbed on a PCI film. The S(^{1}D) TOF spectrum from ASW adsorption was also measured. The obtained TOF distributions were nearly independent of the ice surface morphology and represented by a combination of fast and slow components. The TOF spectra, $I(a, r, t)$, were simulated by a composite of normalized TOF functions, $I_G(t)$ and $I_{MB}(t)$. These functions correspond to a Gaussian energy distribution, $P_G(E_T)$, and a flux-weighted Maxwell–Boltzmann translational energy distribution, $P_{MB}(E_T)$, respectively:

$$I(a, r, t) = aI_G(t) + (1 - a)I_{MB}(t) \quad (7)$$

$$P_G(E_t) = [w(2p)^{1/2}]^{-1} \exp\left[\frac{-2(E_t - \langle E_t \rangle)^2}{w^2}\right] \quad (8)$$

$$P_{MB}(E_t) = (k_B T_{trans})^{-2} E_t \exp\left[\frac{-E_t}{(k_B T_{trans})}\right] \quad (9)$$

where a is the coefficient, t is the time-of-flight of the photofragment, and w is the energy width. The TOF spectra simulation details are described thoroughly in our previous paper [14].

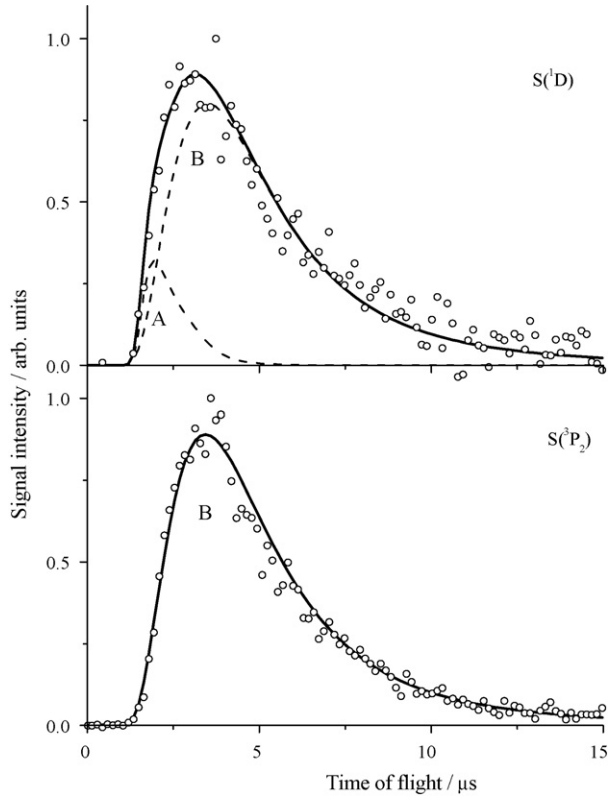

Fig. 2. Time-of-flight spectra of S(^{3}P$_2$) and S(^{1}D) from the 193 nm photodissociation of OCS on a crystalline ice film. Substrate temperature $T_S = 90$ K. The S(^{1}D) spectrum consists of two distributions: a Gaussian distribution marked with A, and a flux-weighted Maxwell–Boltzmann translational energy distribution marked with B. The S(^{3}P$_2$) spectrum consists of a flux-weighted Maxwell–Boltzmann translational energy distribution marked with B. Averaged energies and contributions are listed in Table 1. The time-of-flight spectrum of S(^{3}P$_1$) is almost the same as that of S(^{3}P$_2$).

Channel A in Fig. 2 is fitted to a Gaussian distribution characterized by an average energy of $\langle E_t \rangle = 9.9$ kcal/mol and peak width of $w = 8.5$ kcal/mol, contributing 11% of the total signal. Channel B is fitted to a Maxwell–Boltzmann distribution and is characterized by a translational temperature of $T_{trans} = 1500$ K ($\langle E_t \rangle = 6.0$ kcal/mol), contributing 89% of the total signal. Table 1 summarizes these results.

3.1.3. Time-of-flight spectra and fine-structure branching ratios of S(^3P_J)

The lower panel of Fig. 2 shows a typical S(^{3}P$_2$) atom TOF spectrum from the photodissociation of OCS adsorbed on a PCI film. The TOF spectra of S(^{3}P$_2$) and S(^{3}P$_1$) were nearly identical. The S(^3P_J, $J = 2$, 1) translational temperature is determined to be 1500 K corresponding to and energy of $\langle E_t \rangle = 6.0$ kcal/mol. The TOF spectra of S(^3P_J, $J = 2$, 1) from ASW was also measured, and the results were nearly the same as OCS adsorbed onto PCI. For OCS exposures of 0.3 to 2.3 L, no appreciable change in the TOF profiles was observed.

The fine-structure branching ratios of S(^3P_J) from the photodissociation of OCS adsorbed on a H_2O PCI ice film was obtained using the relative cross sections for two-photon absorption reported by Brewer et al. [18]. The spin-orbit distribution was determined to be $^3P_2$: $^3P_1$: $^3P_0 = 0.97$: 0.03: 0.00, corresponding to a spin-orbit temperature of $T_{spin\text{-}orbit} = 190$ K. On a D_2O PCI film, the distribution was determined to be 0.78: 0.15: 0.07, corresponding to $T_{spin\text{-}orbit} = 570$ K.

3.1.4. Change of time-of-flight spectra after prolonged photoirradiation

As shown in Fig. 3, after prolonged irradiation (typically $>5 \times 10^{17}$ photons), a new TOF component, A′, is observed, which is described by a Gaussian distribution characterized by $\langle E_t \rangle = 18.0$ kcal/mol and $w = 8.5$ kcal/mol. The new A′

Table 1
Averaged translational energies and contributions of the Gaussian and the Maxwell–Boltzmann (M–B) components in the time-of-flight spectra of S(^{1}D) and S(^{3}P$_2$) atoms from the photodissociation of OCS and CS_2 on polycrystalline and amorphous solid water film surfaces and in the gas phase at 193 nm

Ice surface	Sulfur atoms	Fast Gaussian component		Slow M–B component	
		Averaged translational energy, $\langle E_t \rangle$ (kcal/mol)	Contribution (%)	Averaged translational energy, $2RT_{trans}$ (kcal/mol)	Contribution (%)
OCS	^{1}D	9.9 ± 0.8	11 ± 2	6.0 ± 0.8	89 ± 2
	^{3}P$_2$[a]	–	–	6.0 ± 0.8	100
CS_2	^{1}D	12.2 ± 0.8	16 ± 2	4.8 ± 0.8	84 ± 2
	^{3}P$_2$[b]	–	–	6.8 ± 0.8	100

Gas phase	Sulfur atoms	Averaged center-of-mass translational energy			
		$\langle E_t \rangle$ (kcal/mol)	Contribution (%)	$\langle E_t \rangle$ (kcal/mol)	Contribution (%)
OCS[c]	^{1}D	13.8	30	5.3	70
	^{3}P$_2$	29.4/22.3	100	–	–
CS_2[d]	^{1}D	8	100	–	–
	^{3}P$_2$	12	100	–	–

[a] For S(^{3}P$_1$), the average energy is almost the same to that of S(^{3}P$_2$).
[b] For S(^{3}P$_1$) and S(^{3}P$_0$), the average energies are almost the same to that of S(^{3}P$_2$).
[c] Photodissociation wavelength is 223 nm [5]. The quantum yield of S(^{3}P$_2$) formation is very small.
[d] [20].

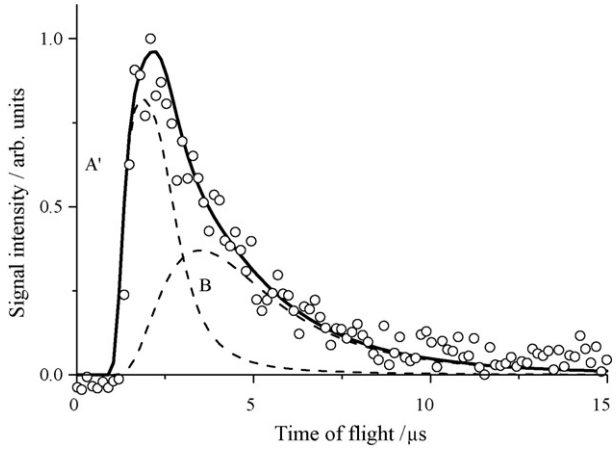

Fig. 3. Time-of-flight spectra of $S(^3P_2)$ from the 193 nm photodissociation of OCS on an amorphous ice film after prolonged photoirradiation ($>5 \times 10^{17}$ photons). This spectrum consists of two distributions: a Gaussian distribution marked with A′ characterized by the averaged translational energy of 18.0 kcal/mol and contribution of 45%, and a flux-weighted Maxwell–Boltzmann translational energy distribution marked with B and characterized by 1500 K or $\langle E_t \rangle = 6.0$ kcal/mol.

component appears in the TOF spectrum of $S(^3P_2)$ of OCS adsorbed to ASW contributing 45% of the total signal. A similar change in the spectrum for PCI was also observed, the new Gaussian component having a slightly lower contribution of 10% of the total signal. These results indicate that new sulfur compounds were produced on the ice films after prolonged photoirradiation, and were subsequently photodecomposed to produce the new TOF component A′. There was, however, no appreciable change in the TOF spectrum for $S(^1D)$ even after prolonged photoirradiation.

3.2. Photodissociation of CS_2 adsorbed on ice films at 193 nm

3.2.1. Preparation of a CS_2 monolayer on ice films

The $S(^3P_2)$ signal intensity was measured as a function of CS_2 exposure on PCI and ASW films. The intensity from the PCI and ASW films increased linearly up to 0.10 and 0.22 L, respectively. The exposure required for monolayer formation on PCI was half of that as required for ASW. In the following sections, experiments were performed with one-monolayer exposures unless stated otherwise.

3.2.2. Time-of-flight spectra of $S(^3P)$ and $S(^1D)$

The TOF spectra of $S(^1D)$ and $S(^3P_J, J = 2, 1, 0)$ produced from the photodissociation of CS_2 adsorbed on ice films were measured. Fig. 4 shows a typical TOF spectra of $S(^1D)$ and $S(^3P_2)$ from PCI. For CS_2 exposures of 0.06–0.4 L, no appreciable change in the TOF profiles of $S(^3P_2)$ was observed. The TOF spectra of $S(^3P_J, J = 2, 1, 0)$ were nearly identical. The TOF spectra of S atoms from ASW were also measured. We found the TOF spectra were independent of the ice surface morphology.

The $S(^1D)$ atom spectra had both fast and slow TOF components. Channel A in Fig. 4 was fitted to a Gaussian

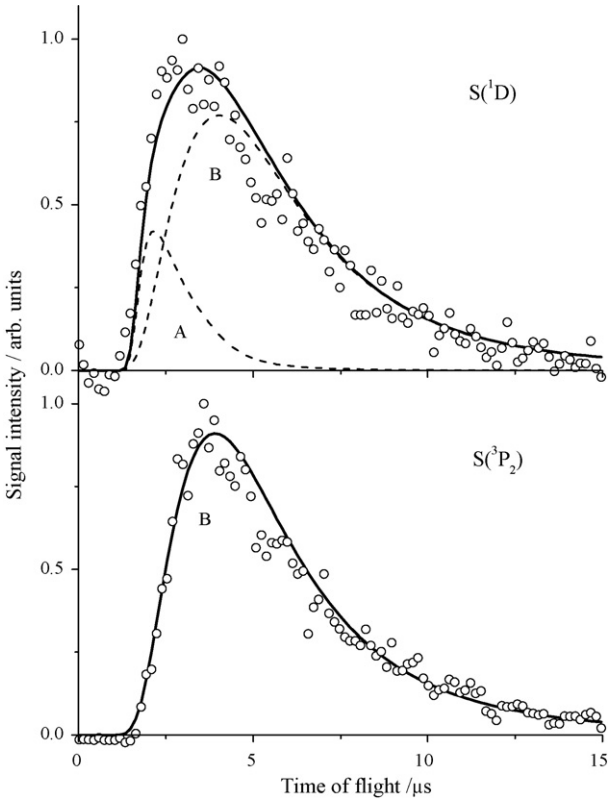

Fig. 4. Time-of-flight spectra of $S(^3P_2)$ and $S(^1D)$ from the 193 nm photodissociation of CS_2 on a crystalline ice film. Substrate temperature $T_S = 90$ K. $S(^1D)$ spectra consist of two distributions: a Gaussian distribution marked by A with $\langle E_t \rangle = 12.2$ kcal/mol, and a flux-weighted Maxwell–Boltzmann translational energy distribution marked by B with $T_{trans} = 1200$ K. $S(^3P_2)$ spectra consist of a flux-weighted Maxwell–Boltzmann translational energy distribution marked by B with $T_{trans} = 1700$ K. Averaged energies and contributions are listed in Table 1. The time-of-flight spectra of $S(^3P_1)$ and $S(^3P_0)$ are almost the same as that of $S(^3P_2)$.

distribution and characterized by $\langle E_t \rangle = 12.2$ kcal/mol and $w = 8.5$ kcal/mol, contributing 16% to the total signal. Channel B was fitted to a Maxwell–Boltzmann distribution and characterized by $T_{trans} = 1200$ K ($\langle E_t \rangle = 4.8$ kcal/mol) contributing 84% to the total signal. In contrast, the TOF distribution of $S(^3P_2)$ is fitted well by a single M–B distribution, which is characterized by $T_{trans} = 1700$ K ($\langle E_t \rangle = 6.8$ kcal/mol). Table 1 summarizes these results.

3.2.3. Fine-structure branching ratios of $S(^3P_J)$ and the change of time-of-flight spectra after prolonged photoirradiation

The fine-structure branching ratio for a H_2O PCI film was determined to be $^3P_2$:$^3P_1$:$^3P_0 = 0.88$:0.09:0.03, and corresponds to a spin-orbit temperature, $T_{spin\text{-}orbit}$, of 350 K. On a D_2O PCI film, the ratio was slightly shifted to 0.83:0.12:0.05, with $T_{spin\text{-}orbit} = 450$ K.

Similar to the photodissociation of OCS, a new Gaussian component characterized by $\langle E_t \rangle = 18.0$ kcal/mol and contributing 29% of the total signal appeared in the $S(^3P_2)$ TOF spectrum for CS_2 adsorbed on ASW and PCI after prolonged irradiation ($>5 \times 10^{17}$ photons) as shown in Fig. 5.

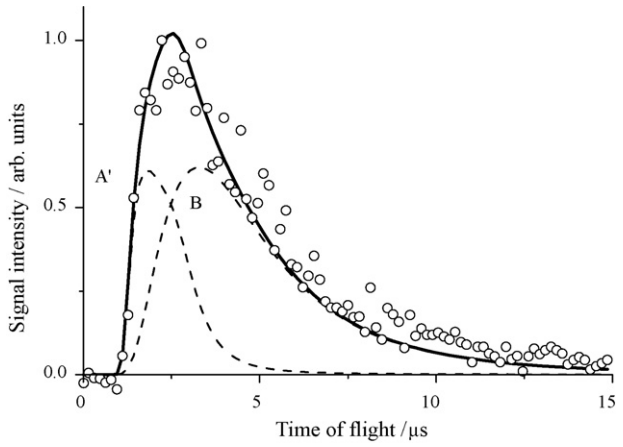

Fig. 5. Time-of-flight spectra of $S(^3P_2)$ from the 193 nm photodissociation of CS_2 on an amorphous ice film after prolonged photoirradiation ($>5 \times 10^{17}$ photons). This spectrum consists of two distributions: a Gaussian distribution marked by A′ characterized with $\langle E_t \rangle = 18.0$ kcal/mol and contribution of 29%, and a flux-weighted Maxwell–Boltzmann translational energy distribution marked by B with $T_{trans} = 1700$ K or $\langle E_t \rangle = 6.8$ kcal/mol.

3.3. Substrate temperature dependence of signal intensity of $S(^3P_2)$ from OCS and CS_2

Photodesorption signal intensities of $S(^3P_2)$ for 0.2 ML of OCS or 0.2 ML of CS_2 on PCI films were measured as a function of the substrate temperature, T_S, at an increasing rate of $1\,K\,s^{-1}$ (Fig. 6). A monotonic decrease of the signal intensities was observed with increasing T_S. The desorption energy of OCS from the ice film surface is smaller than that of CS_2 over the experimental temperature range.

4. Discussion

4.1. Translational energy distributions of $S(^1D)$

Table 1 shows the averaged translational energies of the sulfur photofragments along with those reported previously for the gas phase photodissociation. The translational energy distribution for $S(^1D)$ produced from OCS adsorbed on ice is represented by two components with average energies of 9.9 and 4.5 kcal/mol. The average center-of-mass energies for the fast and slow components of $S(^1D)$ photofragments in the gas phase at 223 nm are 13.8 and 5.3 kcal/mol, respectively [19]. The center-of-mass translational energies in the gas phase would then correspond to the presently observed translational energies for surface photodissociation since the ice film would be the infinitely heavy counterpart. In the gas phase the bimodality was attributed to the parallel and perpendicular transitions to the $^1A'$ and $^1A''$ states, respectively. The TOF spectra for photodissociation of OCS adsorbed on ice could not be obtained from the superposition of these two gas phase components even after the difference in photodissociation wavelength (223 nm/gas versus 193 nm/surface) was taken into account. Leggett et al. reported that for OCS adsorbed on LiF, there was no variation in the photodesorption spectra and there was a lack of evidence for a specific angular distribution, i.e. no distinct parallel and perpendicular transitions [8]. It is reasonable to conclude that the fast atoms emitted from the ice surface represent products of direct $S(^1D)$ photodesorption, whereas the slow atoms which are characterized by a Maxwell–Boltzmann distribution with $\langle E_t \rangle = 6.0$ kcal/mol initially proceed through an energy relaxation process. Alternatively, $S(^1D)$ atoms which are not immediately desorbed from the ice may react with the coadsorbed OCS molecules possibly leading to S_2 and CO as products.

The fast $S(^1D)$ atom translational distribution produced during photodissociation of CS_2 adsorbed to the ice surface ($\langle E_t \rangle = 12.2$ kcal/mol and $w = 8.5$ kcal/mol) is slightly greater but comparable to the gas phase photodissociation energy distribution ($\langle E_t \rangle = 8$ kcal/mol with $w =$ ca. 6 kcal/mol) [20]. The slow $S(^1D)$ component is characterized by a Maxwell–Boltzmann distribution with $\langle E_t \rangle = 4.8$ kcal/mol, which is attributed to photodissociated $S(^1D)$ atoms that collide with the ice surface and are translationally relaxed prior to being ejected into the gas phase.

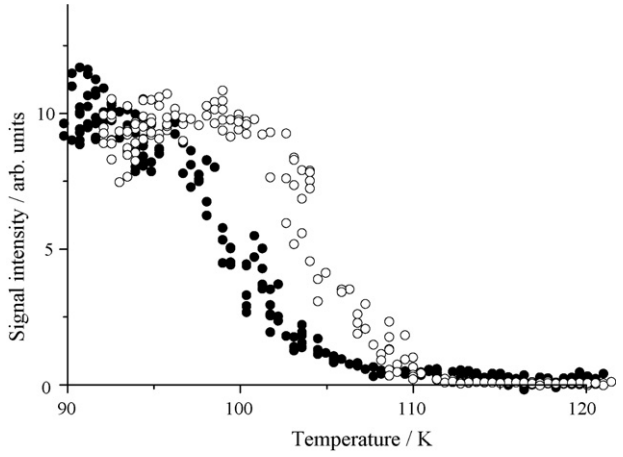

Fig. 6. Temperature dependence of $S(^3P_2)$ signal intensities from the 193 nm photodissociation of OCS (filled circle) or CS_2 (open circle) on crystalline ice films. The signal intensities are normalized to those at 90 K, respectively. The substrate temperature was increased at a rate of $1\,K\,s^{-1}$.

4.2. Translational energy distributions of $S(^3P_J)$ photofragments

The formation of $S(^3P_J)$ from adsorbed OCS photodissociation is attributed to either (a) intersystem crossing to a dissociative triplet state after electronic excitation of the parent OCS molecule or (b) collisional intersystem crossing of the photoproduced $S(^1D)$ to $S(^3P_J)$.

$$\text{(a)}\quad OCS + h\nu \rightarrow OCS^*(2^1A' \text{ and } 2^1A'') \rightarrow OCS^*(\text{triplet}) \rightarrow CO + S(^3P_J) \qquad (2')$$

$$\text{(b)}\quad OCS + h\nu \rightarrow OCS^*(2^1A' \text{ and } 2^1A'') \rightarrow OC + S(^1D) \qquad (1')$$

$$S(^1D) \text{ on ice surface} \rightarrow S(^3P_J) \qquad (10)$$

If the intersystem crossing were due to reaction (10), $S(^1D)$ atoms produced on ASW would relax to a greater degree than

$S(^1D)$ atoms produced on PCI. However, the translational temperature of $S(^3P_J, J=2, 1)$ from ASW was 1500 K, and its contribution to the total signal is almost the same as the contribution from PCI. Hence, we suspect that the $S(^3P)$ atoms were produced during the primary photodissociation process (a) via an electronic intersystem crossing. The speed and angular distributions of $S(^1D)$ and $S(^3P_2)$ fragments observed in the gas phase photo-dissociation experiments suggests that channels (1) and (2) arise from the same singlet states $2^1A'$ and $2^1A''$ [5]. The yield of the triplet S atom is very small in the gas phase. On ice films, however, the interaction between the electronically excited OCS and ice surfaces enhances the intersystem crossing efficiency and the formation of $S(^3P)$ becomes more appreciable. The average translational energy of $S(^3P_2)$ produced from reaction (2) on ice films is only 6.0 kcal/mol, while the average translational energy from the same reaction in the gas-phase is about four times higher. Suggesting there is an efficient energy transfer process between the photoexcited OCS and the ice surface to which it is adsorbed. A similar interaction was observed in our previous study on the UV photodissociation of Cl_2 adsorbed on ice surfaces [21]. Since the interaction of Cl_2 with H_2O is relatively strong, the potential curves are distorted and the adiabaticity of the Cl_2 potential curves is varied.

Leggett et al. reported the UV photodissociation of OCS adsorbed on a LiF (0 0 1) substrate at 116 K. The translational energy distribution of $S(^3P)$ was well represented by a Maxwell–Boltzmann distribution with an average translational energy of 4.2 kcal/mol [8]. This is a similar translational energy distribution to what we have observed for OCS adsorbed on an ice film, although the photoexcitation process of OCS adsorbed on the LiF crystal is mediated by a long range F-center electronic energy transfer process. The fact that the $S(^3P)$ photofragments from OCS adsorbed to ice films and LiF surfaces have similar translational energy distributions suggests that the energy transfer from electronically excited OCS* to any surface occurs efficiently and is not due to a specific surface structure, i.e. the efficient energy transfer is due to the molecule being adsorbed and thus closely associated with a relatively massive energy sink.

The center-of-mass translational energy distribution for $S(^3P)$ atoms from the photodissociation of CS_2 in the gas phase lies in the range of 0–40 kcal/mol with and average energy, $\langle E_t \rangle = 12$ kcal/mol, while the energy distribution from photodissociation of CS_2 adsorbed on ice surfaces is 6.8 kcal/mol. Energy transfer to the ice surface is quite effective due to strong interaction of the electronically excited CS_2 with ice surface, similar to the discussion above for OCS*. Both the intersystem crossing from the photoprepared $CS_2^*(^1B_2)$ state to dissociative triplet state(s) and the energy transfer to ice surface were efficient.

4.3. Fine-structure branching ratios of $S(^3P_J)$

The spin-orbit temperatures, $T_{\text{spin-orbit}}$, of $S(^3P_J)$ from the photodissociation of OCS and CS_2 on ice films are much lower than the corresponding translational temperatures; $T_{\text{spin-orbit}}$ for OCS was 190 K for H_2O and 570 K for D_2O. $T_{\text{spin-orbit}}$ for CS_2 was 350 K for H_2O and 450 K for D_2O. During the gas phase photodissociation ($\lambda = 193$ nm), the fine-structure branching ratio of $S(^3P_J)$ corresponds to $T_{\text{spin-orbit}} = 700$ K and is also much lower than the translational temperature [22]. The spin-orbit distribution is primarily correlated with the adiabaticity of the electronically excited parent molecule's potential curves.

This isotope effect of water ice may be due to the difference in the lattice vibration energies of solid H_2O and D_2O. The spin-orbit energy differences between $S(^3P_J, J=1, 0)$ and $S(^3P_2)$ are 49 and 71 meV, respectively, for H_2O and D_2O ice films. In this low energy region, the inelastic neutron scattering spectra of H_2O and D_2O ice films were reported, and well-separated librational modes that spread from 68 to 125 meV for H_2O and from 49 to 88 meV for D_2O were observed [23]. This isotopic energy differences will influence the degree of energy transfer between $S(^3P_J)$ and the lattice vibrational modes of the ice film. If the energy transfer occurs via resonance conditions, $S(^3P_J)$ adsorbed on D_2O is expected to have a greater degree of relaxation than on H_2O. However, this was not the case for the photodissociation of OCS and CS_2 on ice films. These results support the conjecture that the formation of $S(^3P_J)$ from OCS is attributed to the intersystem crossing of the electronically excited parent molecule to a dissociative triplet state via Reaction (2).

4.4. Production of sulfur dimer molecules by reactions of $S(^1D)$ with OCS and CS_2

The TOF signal intensity from surface photodissociation is represented by [number density of parent molecules adsorbed onto the ice film] × [detachment probability of sulfur atom]. The surface area of ASW has been reported to be about six times larger than that of PCI [24]. Based on the data of Fig. 1, the effective surface area of ASW is roughly two times larger than that of PCI in the present experiments. In spite of this, the $S(^3P_2)$ signal intensity from OCS on ASW at the 1.4 L exposure (one monolayer coverage) was one third of that from PCI at the 0.6 L exposure. (Fig. 1) The nascent S atoms could be trapped molecules in the micropores of the ASW film and then subsequently react with coadsorbed, intact parent molecules, The effective photodetachment probability of the sulfur atoms from ASW was lower than that from PCI by an order of magnitude and is the explanation of the lower $S(^3P_2)$ signal intensity from OCS on ASW as compared to PCI even though ASW has a greater surface area.

Sulfur dimer molecules are the most plausible reaction product candidate and were observed to be produced via the reaction of the photolytically produced sulfur atoms with coadsorbed OCS on a LiF substrate via reactions (3) and (4) [8,9]. Also, sulfur dimer formation was observed during photolysis of $(OCS)_n$ cluster [4] and under slow flow conditions [10], via reaction (3) because the reaction of $S(^1D)$ with OCS is fast. The contribution of a new Gaussian component A′ in the TOF spectrum of Fig. 3 from ASW was 45%, which was three times larger than observed for PCI (10%). The probability of the S atom photofragments being adsorbed more strongly and subsequently reacting with OCS in the micropores of the ASW film surface is higher than that on the relatively smooth PCI surface. Thus S_2 molecules

were produced to a greater degree on the ASW ice film. The recombination of S atoms is another possible production pathway.

Since the translational energies of the Gaussian components A′ in Figs. 3 and 5 are the nearly identical, the same secondary product is expected for both CS_2 and OCS reactions. A theoretical calculation on the reaction between S and CS_2 to produce a sulfur dimer, reaction (11), was reported using the 6-31G* *ab initio* self-consistent-field method [25]. Laser induced fluorescence detection of S_2 was also reported for the following reaction [26]:

$$S(^1D) + CS_2 \rightarrow CS_3 \rightarrow S_2 + CS, \quad \Delta H = -23\,\text{kcal/mol} \tag{11}$$

4.5. Interaction between ice surface and adsorbates

The exposure of CS_2 required for monolayer coverage was about six times smaller than that of OCS. This result suggests that the interaction of CS_2 with water molecules of the ice surface is stronger than that of OCS (i.e. the sticking probability of CS_2 is higher than OCS at 90 K). This tendency is also observed at temperatures up to 110 K in Fig. 6. Based on our TOF results, the sulfur atoms of OCS and CS_2 may directly interact with water molecules at the ice surface. Since the S atoms of the adsorbed molecules point towards the ice surface, the contributions of the slow M–B component of sulfur atoms in Table 1 were much larger than the fast Gaussian component. The fact that two S atoms of CS_2 interact with ice surface while one S atom for OCS explains (a) the larger sticking coefficient of CS_2 in Fig. 6 and (b) the strongly relaxed M–B components in the TOF spectra.

5. Conclusions

The photodissociation mechanism of OCS and CS_2 adsorbed on amorphous and crystalline ice films have been studied by monitoring the TOF spectra of $S(^1D)$ and $S(^3P_J)$ atoms produced via photodissociation. The interaction of CS_2 with the ice surfaces is stronger than that of OCS based on the measurements of the relative sticking probabilities. The interaction between OCS and ice films enhances a triplet dissociation channel producing $S(^3P_J) + CO$. The primary photoproduced S atoms react with coadsorbed parent molecules, OCS or CS_2, to form S_2 as a secondary product. The recombination of S atoms is also a plausible pathway. The micropore structures on the surface of the amorphous solid water film provide regions that enhance the production of sulfur dimer secondary product molecules as compared to smooth polycrystalline ice films. These observations are have implications for astrochemical sulfur chemistry.

References

[1] M.H. Moore, B. Donn, R.L. Hudson, Icarus 74 (1988) 399–412.
[2] R.J.A. Grim, J.M. Greenberg, Astron. Astrophys. 181 (1987) 155–168.
[3] M.F. A'Hearn, P.D. Feldman, D.G. Schleicher, Astrophys. J. 274 (1983) L99–L103.
[4] N. Sivakumar, G.E. Hall, P.L. Houston, J.W. Hepburn, I. Burak, J. Chem. Phys. 88 (1988) 3692–3708.
[5] H. Katayanagi, Y. Mo, T. Suzuki, Chem. Phys. Lett. 247 (1995) 571–576.
[6] Y. Sato, Y. Matsumi, M. Kawasaki, K. Tsukiyama, R. Bersohn, J. Phys. Chem. 99 (1995) 16307–16314.
[7] R. Atkinson, D.L. Baulch, R.A. Cox, J.N. Crowley, R.F. Hampson, R.G. Hynes, M.E. Jenkin, M.J. Rossi, J. Troe, Atmos. Chem. Phys. 4 (2004) 1461–1738.
[8] K. Leggett, J.C. Polanyi, P.A. Young, J. Chem. Phys. 93 (1990) 3645–3658.
[9] St.J. Dixon-Warren, K. Leggett, M.S. Matyjaszczyk, J.C. Polanyi, P.A. Young, J. Chem. Phys. 93 (1990) 3659–3672.
[10] R.C. Richter, A.R. Rosendahl, A.J. Hynes, E.P.F. Lee, J. Chem. Phys. 109 (1998) 8876–8886.
[11] D. Xu, J. Huang, W.M. Jackson, J. Chem. Phys. 120 (2004) 3051–3054.
[12] T.N. Kitsopoulos, C.R. Gebhardt, T.P. Rakitzis, J. Chem. Phys. 115 (2001) 9727–9732.
[13] S.C. Yang, A. Freedman, M. Kawasaki, R. Bersohn, J. Chem. Phys. 72 (1980) 4058–4062.
[14] A. Yabushita, Y. Inoue, T. Senga, M. Kawasaki, S. Sato, J. Phys. Chem. B 106 (2002) 3151–3159.
[15] M. Kawasaki, Appl. Surf. Sci. 135 (1998) 115–120.
[16] S. Sato, D. Yamaguchi, K. Nakagawa, Y. Inoue, A. Yabushita, M. Kawasaki, Langmuir 16 (2000) 9533–9538.
[17] H.H. Huang, Z. Zou, X. Jiang, W.Y. Chan, G.Q. Xu, J. Phys. Chem. B 101 (1997) 8164–8168.
[18] P. Brewer, N. van Veen, R. Bersohn, Chem. Phys. Lett. 91 (1982) 126–129.
[19] T. Suzuki, H. Katayanagi, S. Nanbu, M. Aoyagi, J. Chem. Phys. 109 (1998) 5778–5794.
[20] W.S. McGivern, O. Sorkhabi, A.H. Rizvi, A.G. Suits, S.W. North, J. Chem. Phys. 112 (2000) 5301–5307.
[21] A. Yabushita, M. Kawasaki, S. Sato, J. Phys. Chem. A 107 (2003) 1472–1477.
[22] I.M. Waller, J.W. Hepbern, J. Chem. Phys. 87 (1987) 3261–3268.
[23] A.I. Kolesnikov, J. Li, S.F. Parker, R.S. Eccleston, C.-K. Loong, Phys. Rev. B 59 (1999) 3569–3578.
[24] S. Sato, personal communication.
[25] R.D.J. Froese, J.D. Goddard, J. Chem. Phys. 96 (1992) 7449–7457.
[26] S.P. Sapers, N. Andraos, D.J. Donaldson, J. Chem. Phys. 95 (1991) 1738–1745.